Helical Molecular Programming: Supramolecular Double Helices by Dimerization of Helical Oligopyridine-dicarboxamide Strands

Volker Berl,[a, b] Ivan Huc,*[c] Richard G. Khoury,[a] and Jean-Marie Lehn*[a]

Abstract: Helically preorganized oligopyridine-dicarboxamide strands are found to undergo dimerization into double helical supramolecular architectures. Dimerization of single helical strands with five or seven pyridine rings has been characterized by NMR and mass spectrometry in various solvent/temperature conditions. Solution studies and stochastic dynamic simulations consistently show an increasing duplex stability with increasing strand length. The double helical structures of three different dimers was characterized in the solid phase by X-ray diffraction analysis. Both aromatic stacking and hydrogen bonding contribute the double helical arrangement of the oligopyridine-dicarboxamide strand. Inter-strand interactions involve extensive face-to-face overlap between aromatic rings, which is not possible in the single helical monomers. Most hydrogen bonds occur within each strand of the duplex and stabilize its helical shape. Some inter-strand hydrogen bonds are found in the crystal structures. Dynamic studies by NMR as well as by molecular modeling computations yield structural and kinetic information on the double helices and on monomer–dimer interconversion. In addition, they reveal the presence of a spring-like extension/compression as well as rotational displacement motions.

Keywords: helical structures · conformation analysis · hydrogen bonds · self-assembly · supramolecular chemistry

Introduction

Whilst *single* helical conformations are found in a variety of natural and synthetic polymers, very few *double* helical structures based on the recognition between the constituent strands have been identified. In DNA, RNA, and nucleic acid analogues such as PNA,[1] selective A–T(U) and G–C base pairing connects the strands of right- and left-handed double helices. The bacterial membrane ion channel Gramicidin[2] and other peptides[3] composed of amino acids with alternating L and D configurations dimerize to form antiparallel β-ribbons which coil into double helices of right- or left-handed helical sense. At a larger scale, fibrous, and sometimes globular proteins form long range coiled coil structures stabilized by extensive interactions between side chains. Thus, α-tropomyosin is a symmetrical coiled coil (pitch = 137 Å) of two parallel right-handed α-helices.[4] Collagen is a right-handed coil (pitch = 86.1 Å) of three distorded polyproline-type left-handed helices.[5] As a rare example of synthetic origin, isotactic poly(methyl methacrylate) has also been shown to adopt a double helical structure in the crystalline state (pitch = 21.0 Å).[6]

Related systems include recently described oligomeric[7] or polymeric[8] self-complementary molecular strands which apparently form linear rather than helical dimers. Organic ligands may assemble into double,[9] triple,[10] and even quadruple[11] helicates upon coordination to transition metals. Double helices also form upon coordination of organic ligands to alkaline metal ions[12] and to anions.[13] In these cases, the assembly is driven by the coordination geometry of the ion and the structure of the ligand rather than by direct inter-strand complementarity. Some covalently linked double-stranded structures have been shown to adopt helical architectures.[14] Finally, natural and synthetic supramolecular fibers may also wrap in multiple helices as observed for example in the structure of microtubules and actin microfilaments,[15] in the structure of stacked arrays of disk-shape molecules,[16] and in the structure of hydrogen-bonded supramolecular networks.[17]

[a] Prof. Dr. J.-M. Lehn, Dr. V. Berl, Dr. R. G. Khoury
Laboratoire de Chimie Supramoléculaire
ESA 7006 of the CNRS, ISIS, Université Louis Pasteur
4 rue Blaise Pascal, 67000 Strasbourg (France)
Fax: (+33) 388 411020
E-mail: lehn@chimie.u-strasbg.fr

[b] Dr. V. Berl
Affiliated institution: Forschungszentrum Karlsruhe GmbH
Institut für Nanotechnologie, Postfach 3640
76021 Karlsruhe (Germany)

[c] Dr. I. Huc
Institut Européen de Chimie et Biologie, ENSCPB
Av. Pey Berland, 33402 Talence Cedex (France)
Fax: (+33) 557 962226
E-mail: ivan.huc@iecb-polytechnique.u-bordeaux.fr

  0947-6539/01/0713-2810 $ 17.50+.50/0

We have recently reported on a new family of oligoamide strands derived from 2,6-diaminopyridine and 2,6-pyridinedicarboxylic acid. These compounds not only self-organize into single helical conformers, but they reversibly assemble giving rise to double-helical dimers.[18] In the preceding account, we described in detail the folding of the monomeric strands into single helices.[19] Herein, we present solution and solid state studies of the formation and structure of the double helical dimers generated by self-assembly of two pentameric and heptameric strands **1**–**5** (Figure 1 and Scheme 1).

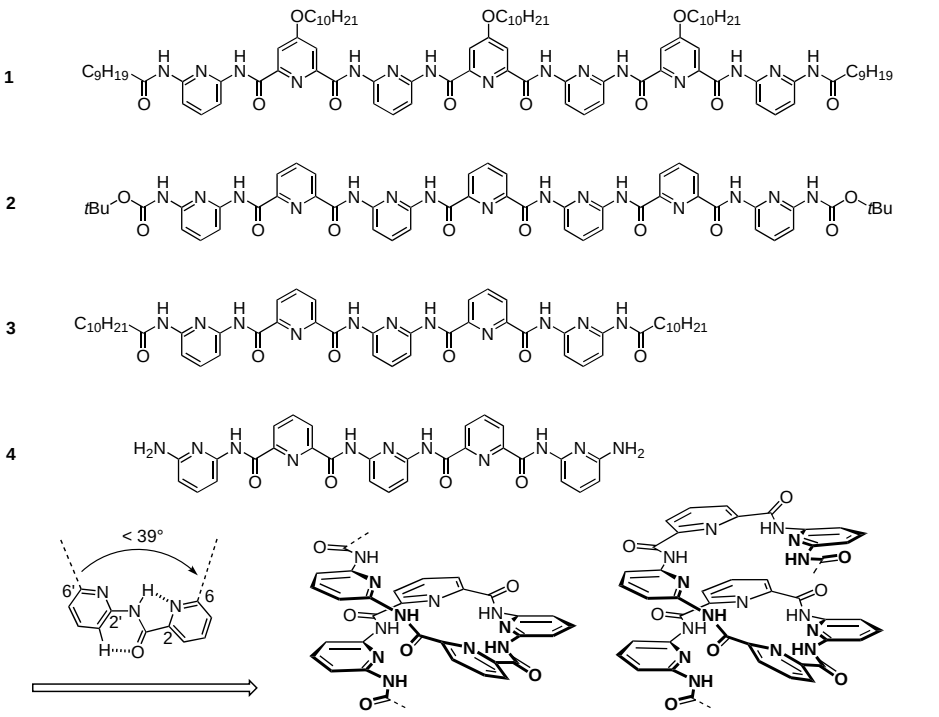

Figure 1. Structure of molecular heptameric strands **1** and **2**, and pentameric strands **3** and **4;** intramolecular hydrogen bonding leading to the folding of the strands into a helical structure. Helices from pentamers extend to over one turn. Helices from heptamers extend to one and a half turns.

Component molecular strands: Experiments and molecular modeling calculations have shown that intramolecular hydrogen bonding within the oligomeric strands **1**–**5** favors a helical shape of the molecules. Single helices have been observed in the solid and in dilute solutions. In pentamers and heptamers, coiling extends to one turn and nearly one-and-half turns, respectively (Figure 1).[18, 19]

Abstract in French: *Des brins moléculaires de type oligopyridine-dicarboxamide préorganisés en hélice se dimérisent en architectures supramoléculaires en double hélice. La dimérisation de brins hélicoïdaux simples ayant cinq ou sept cycles pyridiniques a été caractérisée par RMN et spectrométrie de masse dans différentes conditions de solvant et de température. Les études en solution et des simulations dynamiques stochastiques révèlent une augmentation de la stabilité du duplex avec l'accroissement de la longueur du brin. La structure en double hélice de trois différents dimères a été déterminée en phase solide par diffraction des rayons X. A la fois des interactions d'empilement et des liaisons hydrogène entre les brins contribuent à la stabilité de l'arrangement en double hélice du brin oligopyridine-dicarboxamide. Les interactions inter-brin mettent en jeu un important recouvrement face-à-face entre noyaux aromatiques, qui ne peut pas se faire dans les monomères à simple brin. La plupart des liaisons hydrogène se font au sein d'un brin donné et stabilisent sa structure hélicoïdale. Quelques liaisons hydrogène inter-brins sont présentes dans les structures cristallines. Des études dynamiques à la fois par RMN et par modélisation moléculaire fournissent des données structurales et cinétiques sur les doubles hélices et sur l'interconversion monomère–dimère. De plus, elles révèlent la présence de mouvements de ressort extension/compression et de déplacement rotationnel.*

Depending on their solubility and their tendency to grow single crystals suitable for X-ray diffraction analysis, the five compounds were used in solution or solid state studies. The diamine pentamer **4** is insoluble in solvents other than DMSO and was used only in the solid state studies. Its didecanoyl derivative **3** as well as heptamers **1** and **5** which bear several alkyl residues are highly soluble in chlorinated and aromatic solvents, and even in pure alkanes for **5**. These compounds proved to be poorly crystalline and were used in the solution studies. Heptamer **2** presented a good compromise between solubility and crystallinity, and could be studied in solution and in the solid.

The synthesis of these compounds was straightforward. The pentamers were prepared in one or two steps, and the heptamers in three steps from the corresponding diaminopyridines and pyridine dicarboxylic esters.[19] The synthesis of heptamer **5** is depicted in Scheme 1. The starting dimethyl 4-decyloxy-2,6-pyridinedicarboxylate (**6**) and 4-decyloxy-2,6-diaminopyridine (**7**) were obtained from chelidamic acid using standard procedures (see Experimental Section).

Formation of supramolecular double helices in solution: The existence of well-defined aggregates of the pyridine-amide oligomeric strands was first recognized from ^{1}H NMR spectra of heptamer **1**. At 0.91 mM in $CDCl_3$, the NMR spectrum is sharp and was assigned to a single helical monomer (Figure 2a).[19] Upon concentrating, these signals do not shift but a second set of signals appears indicating the presence of another species in slow exchange on the NMR time scale with the monomeric entity (Figure 2). Heating an 8.2 mM solution causes an increase of the proportion of the latter, up to 98 % at 55 °C, without any coalescence. The concentration and

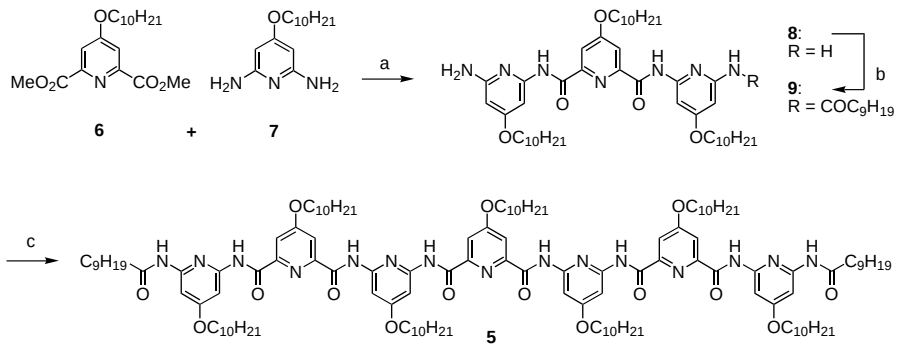

Scheme 1. Synthesis of **5**: a) *n*BuLi, THF, −78 °C; b) $C_9H_{19}COCl$ (1 equiv), NEt_3, THF, 0 °C; c) 4-decyloxy-2,6-pyridinedicarbonyl dichloride (0.5 equiv), NEt_3, THF, 0 °C.

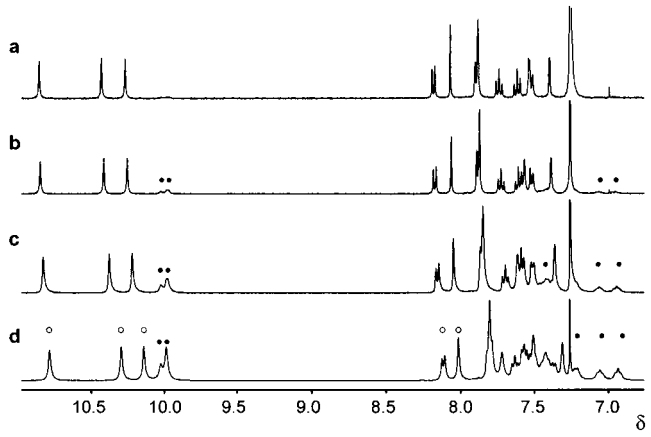

Figure 2. 400 MHz ^{1}H NMR spectra of $CDCl_3$ solutions of **1** at various concentrations at 25 °C. Some of the signals assigned to the monomer (○), and to the dimer (●) are labelled. a) 0.91 mM; b) 2.7 mM; c) 8.2 mM; d) 24.5 mM.

temperature dependence between the two species suggests that the new signals correspond to an aggregate of two or more helical monomers. The exchange is clearly visible on the ^{1}H NOESY spectra where cross-peaks are observed between each signal of the monomer and each signal of the aggregate. This allows, for example, to confirm that the broad triplets observed at $\delta = 7.06$ and 6.94 correspond to the signals of the protons in position 4 of the 2,6-diaminopyridine rings in the aggregate. Saturation transfer experiments yielded an exchange rate of 8.7 s^{-1} at 25 °C.

The proportions between the monomer of **1** and its aggregate at different concentrations (1–25 mM; see Figure 2) are consistent with a dimerization constant K_{dim} of 25–30 $L\,mol^{-1}$ in $CDCl_3$ at 25 °C. The NMR spectra of heptamer **2** feature similar concentration dependence and slow exchange between monomeric and aggregate species (not shown). The proportions between these signals are in agreement with a dimerization constant of 110–120 $L\,mol^{-1}$ in $CDCl_3$ at 25 °C. The NMR spectra of heptamer **5** suggest that this compound undergoes a similar dynamic equilibrium (Figure 3). In this case, however, the aggregate remains the major species at concentrations as low as 300 μM. Quantitative analysis of the NMR data led to a dimerization constant $K_{dim} = 6.5 \times 10^4$ $L\,mol^{-1}$ in $CDCl_3$, which is three orders of magnitude higher than that of **1** in the same solvent.[20] The much higher stability of the dimer of **5** compared with that of **2** may result from interactions between the side chains as well as an increase in interactions between the aromatic rings due to the donor character of the decyloxy substituent in **5**.

That these aggregates are indeed dimers was shown by FAB mass spectrometry. Both monomer and dimer peaks are present on mass spectra taken using a nitrophenyloctylether matrix (data not shown). For compound **1**, the intensity of the dimer peak is low and its assignment to an ion-molecule adduct cannot be ruled out. For compound **5**, however, the more stable dimer survives the relatively harsh ionization conditions of the FAB-MS spectrometry, and its peak intensity (4463.7 $g\,mol^{-1}$) is 35% against 100% for the monomer (2231.4 $g\,mol^{-1}$). No other aggregates and minor fragments peaks (< 5%) are observed in these spectra.

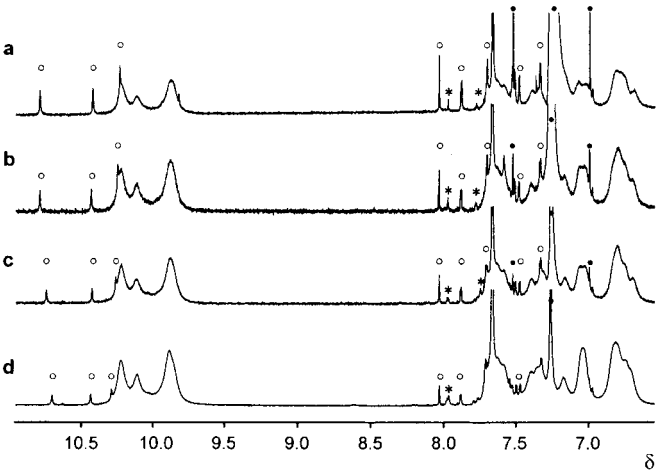

Figure 3. 400 MHz ^{1}H NMR spectra of $CDCl_3$ solutions of **5** at various concentrations at 25 °C. Some of the signals assigned to the monomer (○), and dimer (●) are labelled. a) 0.30 mM; b) 0.91 mM; c) 2.7 mM; d) 8.2 mM.

The NMR signals of the dimers are overall strongly shielded compared with the monomeric species, suggesting that intermolecular π–π aromatic stacking is important in the aggregation process which seems reasonable for such compounds containing several aromatic residues. However, simple stacking of independent helices should be fast on the NMR time scale and lead to a mixture of oligomers instead of a well defined aggregate. Instead, the dimerization observed apparently requires considerable conformational changes in the molecules. For these reasons, we hypothesized the formation of a double helix consisting of two intertwined monomeric strands, which would stack all along their length, so that association and dissociation would require at least partial winding and unwinding of the helical monomeric strands (Figure 4). This double stranded helix was clearly characterized in the solid state (see below). In solution, we sought for intermolecular contacts consistent with such a structure on the NOESY spectra, but this was hampered by the numerous correlation signals due to the monomer–dimer exchange.

0947-6539/01/0713-2812 $ 17.50+.50/0 *Chem. Eur. J.* **2001**, *7*, No. 13

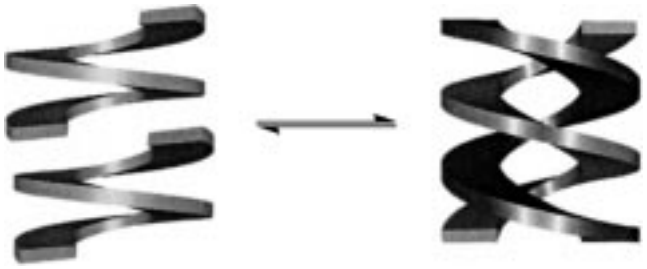

Figure 4. Schematic representation of the interconversion of two helical monomers and a double helical dimer. This corresponds to a spring-like compression/extension of the monomers.

Stability of the double helices in solution: We assessed the stability of the dimers in solution as a function of the strand length, the nature of the solvent, and the presence of water. Pentamer **3** was synthesized in order to compare its aggregation behavior to that of heptamers **1**, **2**, and **5**. The NMR spectra of 4 mM solutions of **3** in $CDCl_3$ or CD_2Cl_2 at 25 °C display only one set of rather broad signals (Figure 5). Upon

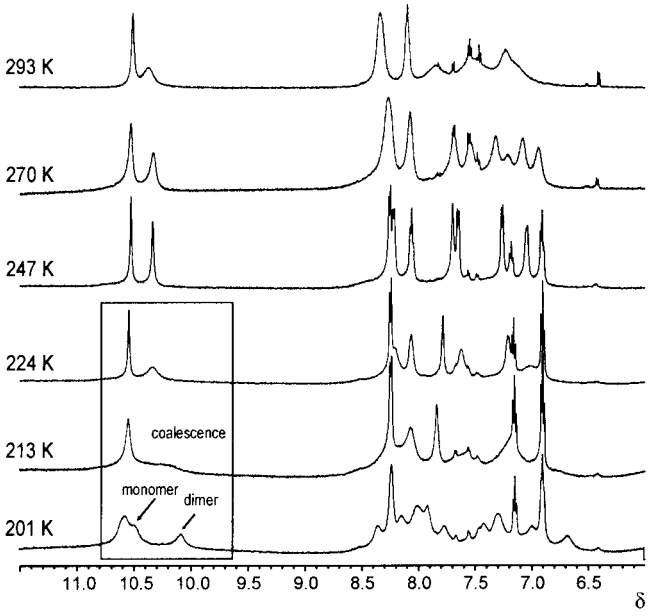

Figure 5. 500 MHz ^{1}H NMR spectra of a 4 mM CD_2Cl_2 solutions of **3** at various temperatures.

concentrating to 50 mM, the signals of the aromatic protons shift up to 0.3 ppm upfield, but no other signals appear on the spectra (data not shown). This suggests that pentamer **3** also aggregates in solution, but that the aggregate is labile on the NMR time scale at 25 °C, and that its signals are averaged with the signals of the monomer. Upon cooling, a coalescence is reached at −60 °C and the signals split below this temperature (Figure 5). At −72 °C in CD_2Cl_2, the proportions between the two sets of signals were shown to vary with concentration in a similar fashion to the variation observed for the heptamers at room temperature. A dimerization of $K_{dim} = 35\ L\,mol^{-1}$ at −72 °C can be calculated. Thus, pentamer **3** apparently forms dimers which are less stable and more labile than the dimers of **1**, **2**, and **5**.

The stability of the dimers proved to be strongly solvent dependent.[18] For compound **1**, K_{dim} was measured at 30, 300, and 22 $L\,mol^{-1}$ in $CDCl_3$, CD_2Cl_2, and 1/9 $CDCl_3/CCl_4$, respectively. For the more stable dimers of **5**, K_{dim} was measured at 6.5×10^4, 1.0×10^5, and 1.6×10^5 in $CDCl_3$, CD_2Cl_2, and $C_2D_2Cl_4$, respectively. These values seem difficult to interpret on the basis of for example solvent polarity. In retrospect, the fact that the water content of the solvents was not controlled prior to the measurements is likely to be responsible for part of these variations. Indeed, the monomer/dimer ratio was shown to vary sharply with the concentration of water in $CDCl_3$ and C_6D_6. As shown in Figure 6, ^{1}H NMR

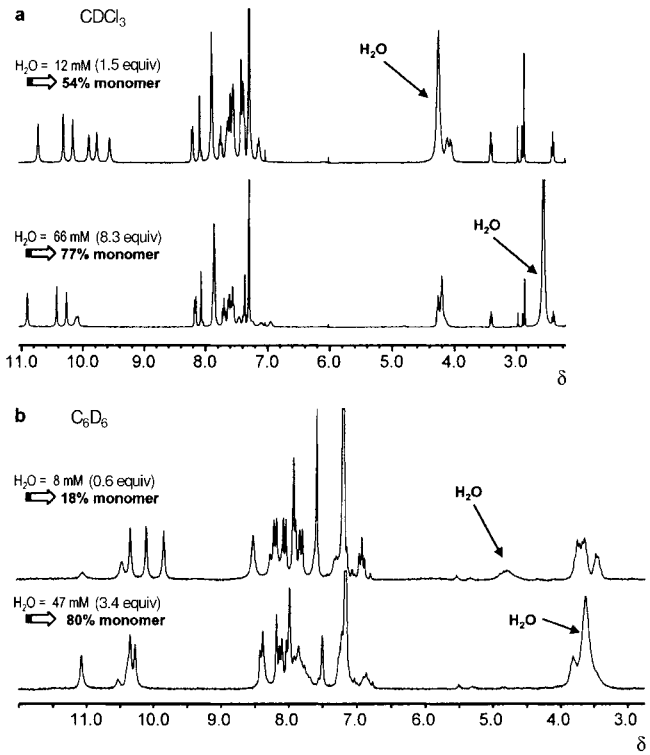

Figure 6. NMR spectra of solutions of **1** in the presence of various amounts of water. a) 8 mM solution of **1** in $CDCl_3$ (400 MHz ^{1}H NMR); b) 13.7 mM solution of **1** in C_6D_6 (200 MHz ^{1}H NMR). The signal assigned to water shifts downfield upon binding the helices. Upon increasing the amount of water, the proportion of single helix increases, and the proportion of double helix decreases.

spectra of **1** in these solvents feature a broad singlet in the $\delta = 2-5$ region, which can be assigned to bound water. That water is bound in solution is not surprising in view of its almost systematic presence in the solid at the polar inner rim of single helices,[19] double helices (see below) and related compounds.[21] Only one water signal is seen on the spectra which indicates a fast exchange on the NMR time scale between bound and unbound water.

The amount of water in solution was varied by drying the solvents and compound **1** prior to sample preparation,[22] followed by a progressive exposure to a humid atmosphere. An increase of the water content resulted in a sharp decrease of the proportion of double helical dimer with respect to the monomer (Figure 6). For example, in a 13.7 mM solution of **1** in C_6D_6, increasing the concentration of water from 8 mM

(0.6 equiv) to 47 mM (3.4 equiv) causes the proportion of dimer to drop from 82% to 20%. This result is important to the interpretation of the presence of water in the double helix structures (see below). Water molecules bind to some of the multiple hydrogen bonding sites of the molecular strands, but apparently do not play the role of coordinating centers which would stabilize the helices in the same fashion transition metals organize ligands in their coordination sphere.[9–12] Instead, hydrogen bonding to water molecules probably competes with intramolecular hydrogen bonding and destabilizes the helical shape required for dimer formation.

Structures of the double helices in the solid state: Solid-state structures of three different double helices were obtained by X-ray diffraction analysis of single crystals. Most importantly, heptamer **2** which was shown to crystallize as a single helix from a DMSO/CH_3CN solvent mixture,[18, 19] crystallizes as a double helical entity from nitrobenzene/heptane (Figure 7).

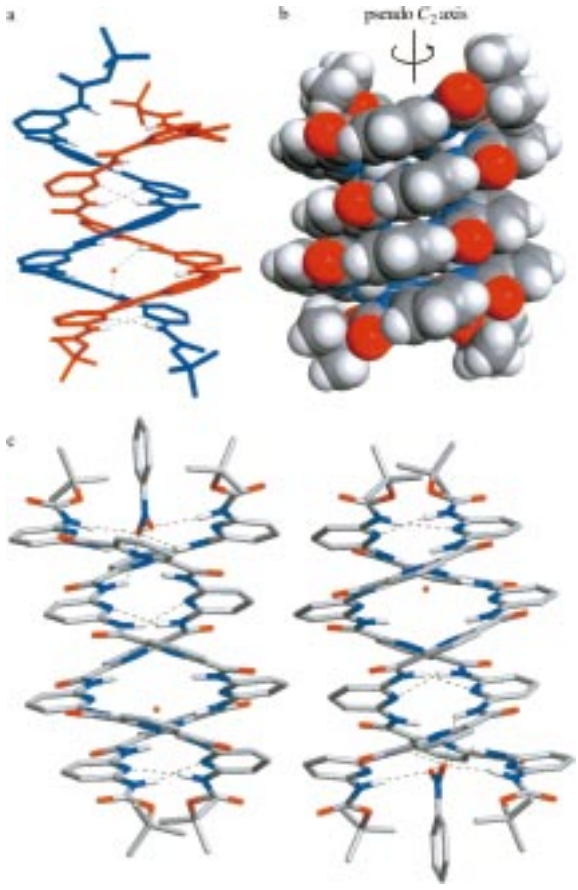

Figure 7. Crystal structure of the double helical dimer of the heptameric strand **2**. In the stick representations, C*H* hydrogens are ommitted for clarity. Dashed lines indicate intermolecular hydrogen bonds between the strands, or between one strand and co-crystallized water or nitrobenzene molecules. Other co-crystallized solvent molecules are not represented. a) Stick representation of a right-handed double helix. The two strands are coded in different colors; b) CPK representation of a different view of the right handed double helix. The two strands are almost super-imposable upon a 180° rotation about the helix axis. c) Stick representation of a neighboring pair of right- and left-handed double helices. In this view, the pinching of the duplex at one end, and its opening at the other end are clearly visible.

This allowed the direct comparison of monomer and dimer structures from the same strand. In addition, two different double-helical structures (quoted $(\mathbf{4})_2\mathbf{A}$ and $(\mathbf{4})_2\mathbf{B}$) were obtained upon crystallizing pentamer **4**, respectively, from DMSO/CH_3CN at 25 °C, and DMSO/CH_3CN at 8 °C in the presence of tetramethylammonium chloride (Figures 8 and 9). All three structures show different crystallographic characteristics (see Table 1) and different double-helical structural patterns.

Table 1. Crystallographic parameters for the structures determined.

Compound	**2** (double helix)	**4** (double helix $(\mathbf{4})_2\mathbf{A}$)	**4** (double helix $(\mathbf{4})_2\mathbf{B}$)
M_W	$C_{51}H_{47}N_{15}O_{10}\cdot 3(C_6H_5NO_2)\cdot(H_2O)$	$C_{29}H_{23}N_{11}O_4\cdot 0.7(C_2H_6SO)\cdot(H_2O)$	$C_{29}H_{23}N_{11}O_4$
crystallizing solvent/	nitrobenzene/	DMSO/	DMSO/
precipitant	heptane	acetonitrile	acetonitrile in the presence of NMe_4Cl
crystal dimensions [mm]	$0.18\times0.15\times0.15$	$0.30\times0.21\times0.18$	$0.22\times0.20\times0.18$
color	colorless	colorless	colorless
unit cell	triclinic	monoclinic	orthorhombic
space group	$P\bar{1}$	$C2/c$	$Pbcn$
dimensions			
a [Å]	18.980(4)	21.220(4)	23.039(5)
b [Å]	19.230(4)	17.880(4)	11.340(2)
c [Å]	19.980(4)	16.790(3)	21.010(4)
angles			
α [°]	81.52(3)	90	90
β [°]	75.11(3)	93.79(3)	90
γ [°]	81.59(3)	90	90
V [Å^3]	6926(2)	6352(2)	5489(1)
Z	4	8	8
FW [g mol^{-1}]	1417.38	662.28	589.58
ρ [g cm^{-3}]	1.350	1.384	1.427
scanned θ	$1.0° \le \theta \le 27.01°$	$2.9° \le \theta \le 27.68°$	$1.77° \le \theta \le 27.63°$
total/unique refl.	30136/14924	7621/3732	6267/2197
parameters	1865	450	397
GOF	1.005	1.062	0.942
res. e$^-$ density [e Å^{-3}]	0.600	0.652	0.991
$R1$ (obs)	**0.099**	**0.113**	**0.076**
wR (all)	**0.213**	**0.249**	**0.236**
CCDC Ref.	142811	147336	147337

*Double helix of heptamer **2*** (*Figure 7*): As expected from solution studies, the double-helix structure allows considerable overlap between the aromatic groups of each monomeric helical strand, with an average $\pi-\pi$ stacking distance of 3.5 Å, corresponding to van der Waals contact. In the double helix, aromatic rings are lying above one another in a face-to-face stacking arrangement. This contrasts with the single helices in which aromatic rings lie above amide functions and only slightly overlap.[19] The coulombic and van der Waals forces associated with aromatic stacking thus seem to promote inter-strand attractive interactions.

0947-6539/01/0713-2814 $ 17.50+.50/0 *Chem. Eur. J.* **2001**, *7*, No. 13

Compared to the single helical structure of **2**,[18, 19] the pyridine–pyridine torsional angles within one strand of the double helix are opened up to an average of 25.4° (17.9–34.0°). This results in a nearly two turn duplex, with 16.7 Å in length, in which only four pyridine-amide units are needed per turn. For comparison, the single helices require about 4.5 pyridine-amide units per turn. This corresponds to a spring-like compression/extension motion of each strand upon single/double helix interconversion.

Most hydrogen bonds occur within each strand of the duplex and stabilize their helical shape in same manner as for the single helices. The structure of duplex $(\mathbf{2})_2$ thus contrasts with the structure of DNA, in which hydrogen bonding determines inter-strand recognition, and stacking takes place mainly within each of the two strands. Yet, four direct inter-strand N*H*–N hydrogen bonds are seen at the ends of the duplex $(\mathbf{2})_2$ (3.19–3.32 Å and 3.21 Å), along with two bridging N*H*–O hydrogen bonds (3.01 and 3.09 Å) to a water molecule bound to the polar inner rim of the duplex, which may contribute to the duplex stability (see above for its role in solution). The duplex is slightly pinched at one end, resulting in an opening at the other end filled by a hydrogen-bonded nitrobenzene solvent molecule (Figure 7). Thus, for this helical pattern to propagate along a longer structure than just a heptamer, the nitrobenzene molecule should be expelled and the pinching relaxed.

*First double helix of pentamer **4***: $(\mathbf{4})_2\mathbf{A}$ (Figure 8a). This double helix bears many common features with the preceding structure, and in particular the considerable intermolecular overlap between aromatic groups of each monomeric helical strand. Here again, aromatic rings are lying above one another in a face-to-face stacking arrangement with an average π–π stacking distance of 3.6 Å, corresponding to van der Waals contact. No direct hydrogen bonds are observed between the strands. A careful examination of the positions of the two water molecules bound to the inner rim of the duplex leads to the conclusion that they do not efficiently bridge the two strands (see above for their role in solution).[23] Other water and crystallizing solvent molecules are filling voids in the crystal lattice, and are not involved in direct interactions with the duplex strands.

This structure is highly regular and may be propagated along a longer duplex with barely any structural modification. In the crystal, each duplex of one helical sense is hydrogen-bonded to two duplexes of the other helical sense (Figure 9). These hydrogen bonds involve the terminal amide N*H*s and the most peripheral carbonyl oxygen atoms. This pattern generates undulating ribbons of hydrogen-bonded double helices. Very little aromatic overlap is observed between different duplexes.

*Second "double helix" of pentamer **4***: $(\mathbf{4})_2\mathbf{B}$ (Figure 8b). The same compound **4** yielded a different structure when crystallized from a slightly different medium. Among the seven crystal structures of single or double helices obtained from the oligopyridine-dicarboxamide strands, this structure is the only one which neither includes water nor solvent molecules. The salt present in the crystallizing solvent (Me_4NCl) may possibly have prevented the water from binding to the strands, and promoted inter-strand hydrogen bonding. The structure of $(\mathbf{4})_2\mathbf{B}$ is indeed characterized by multiple (a total of eight) hydrogen bonds between the two strands, depicted in detail in Figure 10.[24] The two strands are in close contact which leaves no space for water molecules to be included. The hydrogen bonds involve the pyridine nitrogens, the amine and the amide hydrogens which all converge towards the helix interior. But they also involve the amide oxygens which diverge from the helix axis. For this to be achieved, both strands are considerably offset, resulting in a very limited aromatic overlap between aromatic rings (see top view in Figure 8b). Another consequence is that this structure is considerably flattened along its helical axis and widened perpendicular to this axis with respect to the helices shown in Figures 7 and 8a. The average dihedral angle between pyridine rings is 18.4° compared with 25.4° and 24.4° for $(\mathbf{2})_2$ and $(\mathbf{4})_2\mathbf{A}$, respectively. In fact this structural pattern may hardly be called double-helical. For instance, it may not be extended to a heptamer without strand divergence or clashes. Nevertheless, it suggests that many variations on the association mode are available to the oligomeric strands,

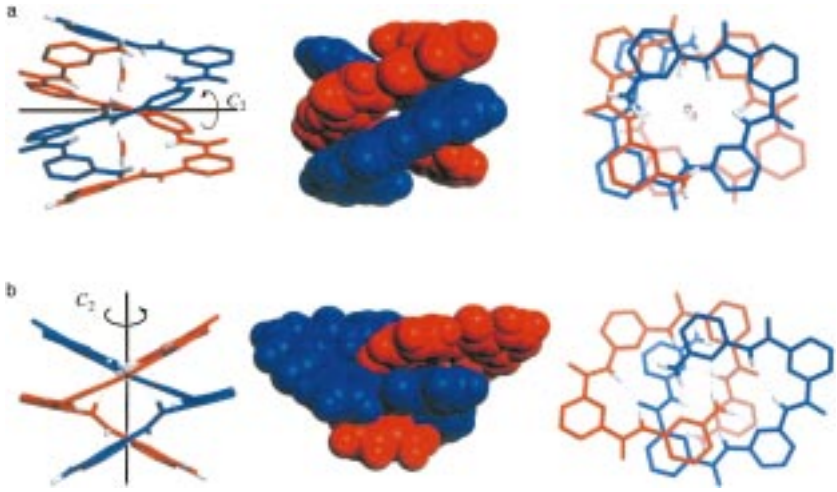

Figure 8. Crystal structures of two different double helical dimers of the pentameric strand **4**. In each duplex, the two strands are coded in different colors. In the stick representations, C*H* hydrogens are ommitted for clarity. a) Structure of $(\mathbf{4})_2\mathbf{A}$ in crystals grown from DMSO/CH_3CN. Co-crystallized solvent other than two molecules of water bound the helix polar inner rim are not represented. The two strands within a duplex may be generated form each other through a crystallographic C_2 symmetry axis which is perpendicular to the helix axis. The top-view (right) shows extensive stacking between aromatic rings of the two strands. b) Structure of $(\mathbf{4})_2\mathbf{B}$ in crystals grown from DMSO/CH_3CN in the presence of Me_4NCl. No solvent or water molecules are found in the crystal lattice. Dashed lines indicate intermolecular hydrogen bonds between the strands. The two strands within a duplex may be generated form each other through a crystallographic C_2 symmetry axis which coincides with the helix axis. The top view (right) shows very poor overlap between aromatic rings of the two strands.

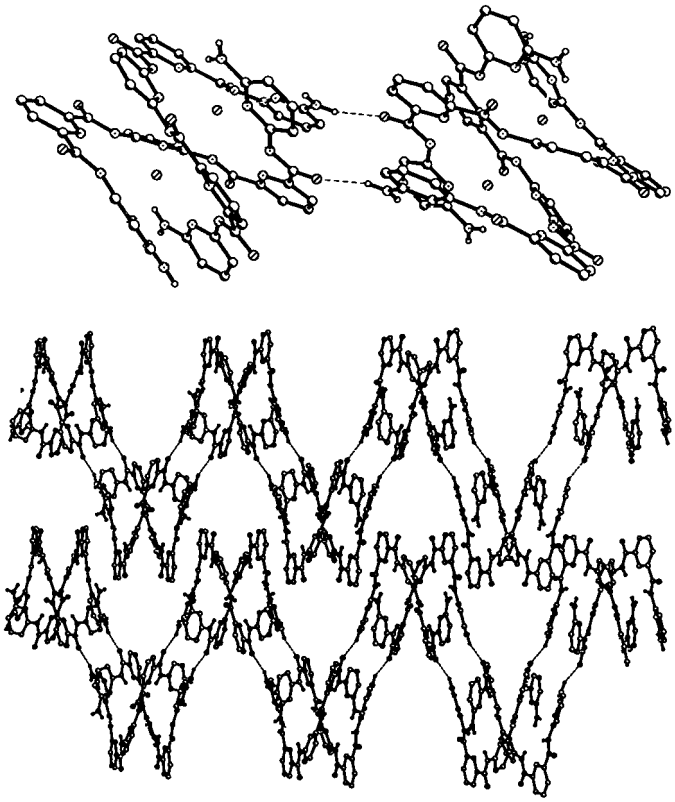

Figure 9. Hydrogen bonding between helical dimers of opposite handedness in the crystal structure of $(\mathbf{4})_2\mathbf{A}$ (see Figure 8a), leading to undulating ribbons.

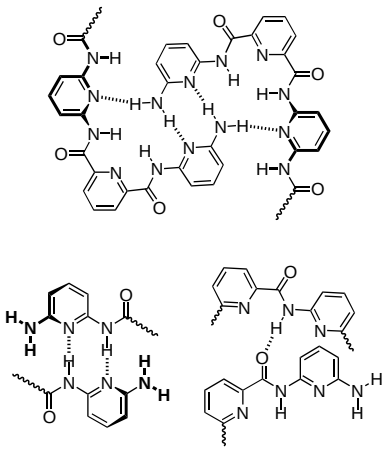

Figure 10. Intermolecular hydrogen bonding patterns present in the crystal structure of $(\mathbf{4})_2\mathbf{B}$ (see Figure 8b).

especially for the shorter ones. The NMR signals of the various dimers observed in solution represent average signals of these structurally different complexes.

Comparative features of the three crystal structures: The three double helical structures, as all the single helical structures obtained, belong to non-chiral space groups. Thus, both right- and left-handed helices are present in the crystal. In all three structures, both strands within a duplex are identical (or almost identical: see below). However, the two ends of each strand are in a different local environment.[25] In the $(\mathbf{2})_2$ duplex for example, one extremity of each strand and not the other one is hydrogen-bonded to a nitrobenzene molecule (Figure 7). However, this dissymmetry is expressed differently from one structure to another. In the $(\mathbf{2})_2$ and the $(\mathbf{4})_2\mathbf{B}$ double helices, the two ends of the duplex are different, but the extremities of the two strands at the same end of the duplex are in the same environment. In the $(\mathbf{4})_2\mathbf{A}$ double helix, the two ends of the duplex are identical, but the extremities of the two strands at the same end of the duplex are in different environments.

This is reflected in the symmetry elements of the duplex structures. In $(\mathbf{2})_2$, the two strands are almost superimposable after a 180° rotation about the helical axis. Slight differences subsist, however, and the helix axis is not a true crystallographic C_2 symmetry axis (Figure 7).[26] In the $(\mathbf{4})_2\mathbf{B}$ duplex, the helix axis is a true crystallographic C_2 symmetry axis (Figure 8b). The $(\mathbf{4})_2\mathbf{A}$ duplex is also crystallographically C_2 symmetrical, but the C_2 axis is perpendicular to the helix axis (Figure 8a).

Other remarkable differences between the three double helical structures are found in the way the aromatic rings overlap. As mentioned before, aromatic stacking in the $(\mathbf{4})_2\mathbf{B}$ duplex is very limited (Figure 8b). In $(\mathbf{2})_2$ and $(\mathbf{4})_2\mathbf{A}$, aromatic rings overlap along the almost entire length of the strands. Since one helical turn involves about four pyridine rings, these double helices may be viewed as four stacks of pyridine rings in a face-to-face arrangement linked by amide groups. The two strands of $(\mathbf{2})_2$ are shifted by two aromatic rings. Owing to the alternation of 2,6-diaminopyridines and 2,6-pyridinedicarbonyls within each strand, this shift causes diaminopyridine rings to stack with other diaminopyridine rings, and pyridinedicarbonyl rings stack with other pyridinedicarbonyl rings. On the other hand, the two strands of $(\mathbf{4})_2\mathbf{A}$ are shifted by only one aromatic ring. In this structure, diaminopyridine rings and pyridinedicarbonyl rings alternately stack onto each other. The cross-section of the $(\mathbf{2})_2$ retains the ellipsoidal shape observed for the helical monomers.[19] Conversely, the cross-section of the $(\mathbf{4})_2\mathbf{A}$ duplex has a circular shape.

In view of the solution and solid state data several hypotheses may be drawn concerning the factors essential to double helix formation:

- The double helical dimers formed from strands of seven or more pyridine rings involve extensive face-to-face aromatic stacking, which is not possible within the helical monomers. Attractive interactions between aromatic rings may operate along the entire duplex structure regardless of its length. It is likely that many forms of these dimers exist, depending on whether the two strands are shifted by 0, 1, 2, or more rings with respect to each other. The interconversion between these binding modes may be viewed as a spiraling sliding motion of the two strands, the dynamics of which have been observed by NMR.[18]
- Direct interstrand hydrogen bonding is possible and is likely to contribute to the duplex stability. However, hydrogen bond formation requires a distortion of the double helix structure and may occur only locally in longer strands.
- inding of water molecules to the polar inner rim of the double helices is not required for dimer formation neither in solution nor in the solid. Excess water causes a

  0947-6539/01/0713-2816 $ 17.50+.50/0 *Chem. Eur. J.* **2001**, *7*, No. 13

dissociation of the strands probably due to a destabilization of the helical conformers, possibly as a result of its competing with intramolecular hydrogen bonding.

Molecular dynamic simulations of the double helices: In order to assess some of the factors discussed above, we have modeled the behavior of the double helices under stochastic dynamic simulations using the program MacroModel.[19] Three double helices were built from strands with 5, 7, and 9 aromatic rings, respectively, on the basis of the structural motif of the $(\mathbf{4})_2\mathbf{A}$ duplex in the crystal. Thus, in these structures, the two strands are shifted by one aromatic ring. Before the stochastic dynamics calculations, a near low energy conformer was found using a steep descent algorithm (SD), the AMBER force field, and GB-SA chloroform simulation. For each structure, several dynamic runs were performed for 1 to 2 ns, at different simulation temperatures.

At a temperature of 300 K, the three helical structures are highly conserved over time (Figure 11). Atoms oscillate slightly around their initial positions. Thermal motion is more pronounced at the strand extremities, but no bonds are allowed a full rotation. No difference in stability was observed in the presence or in the absence of water bound to the helices inner rims.

Motions and rotations gain in amplitude and frequency upon increasing simulation temperature. Higher temperatures *in silico* increase the chance of observing otherwise slow processes during short simulations. The stability of the double helices increase with strand length, which is consistent with solution NMR data. At 700 K all duplexes dissociate within the first 100 ps of simulation (not shown). At 500 K, the pentameric strands rapidly loose their helical structure but they remain in close contact and the dimer does not completely dissociate (Figure 12a). After 360 ps of simulation, a double helical structure is temporarily reached again. Interestingly, this duplex is of left-handed helical sense whereas the starting duplex was right-handed. Thus, with short pentameric strands, the double helix may invert without complete dissociation of the strands. These simulations would suggest that dissociation occurs through simultaneous and progressive unfolding of both strands of the duplex, and not through sliding of the strands along one another in a spiralling motion. Rotations about the pyridine amide nitrogen bonds are frequent during the simulation. Occasionnally, intramolecular hydrogen bonds are disrupted which allow rotation about the pyrdine–carbonyl bonds.

Unlike the pentamers, the heptameric strands remain helical at 500 K (Figure 12b). Thermal motions have much wider amplitudes than at 300 K (Figure 11), and substantial variations from the initial double helical shape are observed after 240 ps. However, the center parts of the strands do not move with respect to each other and large amplitude motions are restricted to the strand extremities which partly unfold and refold. In the same conditions, the structure of a duplex of two nonameric strands is even more conserved (Figure 12c). Low amplitude motions are observed at the strand ends.

Conclusion

The formation of double helices described here results from a sequential, hierarchical process in which the helical folding of a single molecular strand is followed by its dimerization. The first step is brought about by the designed encoding of correct and suitably robust interactional information into the molecular framework. The second step, the dimerization, results from a balance of factors involving the intrinsic stability of the single helical monomer, supramolecular interstand interactions as well as environmental effects acting through their relative influence on the two entities in equilibrium.

The results obtained provide guidelines for stabilizing the dimeric species and thus for programming the self-assembly into double helical structures by the correct design of the monomeric strand. Further refinement towards better control may be obtained by exploring the effect of introducing other structural elements, such as other aromatic groups or other linkers between them. The present entities also offer a framework for arranging peripheral substituents into a double helical array (as in the DNH double helicates[9b]); in particular, one may envisage strands bearing respective

Figure 11. Dynamic simulations at 300 K of three double helices composed from left to right of two pentameric, heptameric, and nonameric strands. In each case, 20 structures recorded during a 40 ps dynamic simulation period are overlaid.

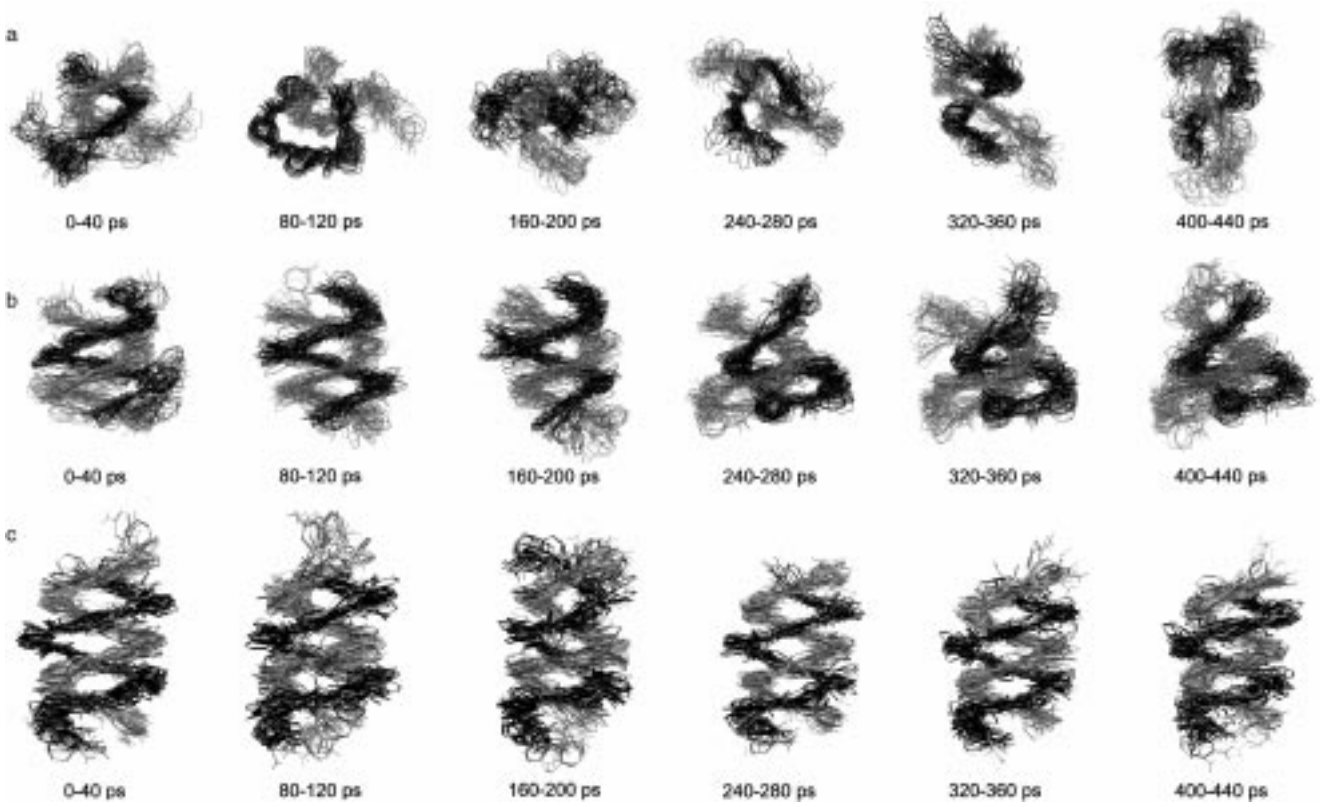

Figure 12. Dynamic simulations at 500 K of three double helices composed of two pentameric a), heptameric b), and nonameric c) strands. The first 480 ps of each simulation are divided 12 periods of 40 ps each; six of them are shown. Structures sampled every 2 ps are overlaid for each period.

electron donor and electron acceptor groups which may form heterostrand dimers. Finally, as already pointed out earlier,[18] the double helices also display molecular motions involving both spring-like extension/compression (with a specific elasticity constant) on dimer formation and rotational sliding of the two partners within the dimers. These present intriguing potential in the design of dynamic supramolecular devices.

Experimental Section

General methods: Compounds **1**, **2**, **4** and **6** were prepared as previously described.[19] THF was distilled over sodium/benzophenone. Triethylamine (Lancaster, 99 %) was used as received. Decanoyl chloride (Aldrich, 98 %) was distilled prior to use. Flash column chromatography was performed using silica gel (Geduran, SI 60 (40 – 63 mm, Merck). Infrared spectra were recorded as thin films on NaCl discs on a Perkin – Elmer 1600 Series FTIR. 400 MHz ^{1}H spectra spectra were recorded on a Bruker Ultrashield Avance 400 spectrometer, 300 MHz ^{1}H NMR and and 75 MHz ^{13}C NMR spectra on a Bruker AM 300 spectrometer, and 200 MHz ^{1}H NMR and 50 MHz ^{13}C NMR spectra on a Bruker SY 200 spectrometer. The solvent signal was used as an internal reference for both ^{1}H and ^{13}C NMR spectra. The following notation is used for the ^{1}H NMR spectral splitting patterns: singlet (s), doublet (d), triplet (t), multiplet (m). FAB-mass spectrometric measurements were performed by the Service de Spectrométrie de Masse, Institut de Chimie, Université Louis Pasteur. Melting points (M.p.) were recorded on a Koffler Heizblock apparatus and are uncorrected. Elemental analyses were performed by the Service de Microanalyse, Institut de Chimie, Université Louis Pasteur.

X-ray crystallography: X-ray diffraction data for compounds **2** (single helix), **2** (double helix), and **4** were collected on a Nonius KappaCCD diffractometer with a graphite monochromatized $Mo_{K\alpha}$ radiation ($\lambda =$ 0.71071 Å), ϕ scans, at 173 K, at the Laboratoire de Cristallochimie, Université Louis Pasteur, Strasbourg. Data were reduced using the Bruker SAINT software. Their structure solution was determined using direct methods and refined (based on F^2 using all independent data) by full matrix least square methods (SHELXTL 97). Hydrogen atoms were included at calculated positions by using a riding model.

Crystallographic data (excluding structure factors) for the structures reported in this paper have been deposited with the Cambridge Crystallographic Data Centre as supplementary publication no. CCDC-147333 ($(\mathbf{2})_2$), CCDC-147336 ($(\mathbf{4})_2\mathbf{A}$), and CCDC-147337 ($(\mathbf{4})_2\mathbf{B}$). Copies of the data can be obtained free of charge on application to CCDC, 12 Union Road, Cambridge CB2 1EZ, UK (fax: (+44) 1223 336-033; e-mail: deposit @ccdc.cam.ac.uk).

Molecular dynamics simulations were performed on a R10000 O2 Silicon Graphics workstation as described before.[19]

2,6-Bis-{[6-(6-decanoylamino-pyridin-2-ylcarbamoyl)-pyridine-2-carbonyl]-amino}-pyridine (3): Decanoyl chloride (25.9 mg, 28.2 μL, 0.1354 mmol, 300 mol %) was added through dry syringe to a solution of **4** (26.7 mg, 0.0452 mmol, 100 mol %) and triethylamine (10.05 mg, 0.0994 mmol, 220 mol %) in dry THF (1 mL). After 3.5 h stirring at r.t., the mixture was heated to 50 °C for 15 minutes, filtered, evaporated to dryness and purified on a column (silica gel, 30 % EtOAc/CH_2Cl_2) to afford **3** (21.6 mg, 53 %) as a gluey gray-white solid. M.p. 160 – 162 °C; IR (thin film): $\tilde{\nu} =$ 3317, 2922, 2839, 1698, 1582, 1514, 1452, 1306, 1244, 1151, 800 cm^{-1}; ^{1}H NMR (500 MHz, CD_2Cl_2, 4 mM, 253 K): $\delta =$ 10.52 (br s, 2H), 10.33 (br s, 2H), 8.25 (d, $^3J =$ 7.3 Hz, 2H), 8.21 (d, $^3J =$ 7.3 Hz, 2H), 8.05 (t, $^3J =$ 7.7 Hz, 2H), 7.70 (br s, 2H), 7.65 (d, $^3J =$ 7.7 Hz, 2H), 7.26 (d, $^3J =$ 7.3 Hz, 2H), 7.18 (t, $^3J =$ 8.9 Hz, 1H), 7.04 (d, $^3J =$ 8.0 Hz, 2H), 6.91 (t, $^3J =$ 8.2 Hz, 2H), 2.24 (t, $^3J =$ 7.7 Hz, 4H), 1.49 (m, 4H), 1.20 (m, 24H), 0.81 (t, $^3J =$ 6.9 Hz, 6H), ^{13}C NMR (50 MHz, $CDCl_3$): $\delta =$ 171.4, 161.8, 161.4, 149.9, 149.5, 148.8, 148.7, 141.2, 140.9, 139.5, 137.5, 126.0, 111.0, 110.2, 109.9; FAB-MS: m/z (%): 898.4 (41) $[M]^+$; HRMS (FAB-MS): calcd for $[C_{49}H_{59}N_{11}O_6+H]$: 898.4728; found: 898.4735.

4-Decyloxy-pyridine-2,6-diamine (7): Diester **6** (2.12 g, 6.22 mmol), and a 1/1 methanol/dioxane solution saturated with anhydrous NH_3 (20 mL) were heated at 120 °C in an autoclave for 12 h. All solvents were removed, and

  0947-6539/01/0713-2818 $ 17.50+.50/0 *Chem. Eur. J.* **2001**, *7*, No. 13

the diamide was dried and used without further purification. A solution of KOH (85%, 4.35 g, 62.2 mmol) in water (23 mL) was cooled to 0–5 °C, and bromine (0.64 mL, 12.45 mmol) was slowly added, followed by the diamide. Dioxane (35 mL) was added to help dissolve the solid. The mixture was stirred 30 min at room temperature, and then heated to 50–55 °C during 45 min. AcOH (3.11 mL) was added and the mixture was heated at 50–55 °C another 20 min. After cooling, KOH was added (2.2 g). The solution was extracted with CH_2Cl_2. The organic phase was evaporated and the residue was chromatographed on silica gel eluting with 5/95 MeOH/EtOAc. The product was recrystallized from $CHCl_3$/cyclohexane. Yield 1.1 g (67%). M.p. 135–136 °C; IR (thin film): $\tilde{\nu}$ = 3341, 3186, 2923, 2851, 1633, 1606, 1576, 1552, 1446, 1384, 1241, 1193, 1025, 786, 726 cm^{-1}; ^1H NMR (400 MHz, $CDCl_3$): δ = 5.48 (s, 2H), 4.11 (br s, 4H), 3.89 (t, ^3J = 6.6 Hz, 2H), 1.71 (m, 2H), 1.28 (m, 14H), 0.89 (t, ^3J = 6.8 Hz, 3H); ^{13}C NMR (100 MHz, $CDCl_3$): δ = 169.4, 159.7, 85.3, 68.3, 32.5, 30.2, 30.0, 29.7, 26.6, 23.3, 14.7; FAB-MS: *m*/*z* (%): 266.1 (100) $[M+H]^+$; HRMS (FAB-MS): calcd for $[C_{15}H_{27}N_3O]$: 266.2232; found: 266.2232.

4-Decyloxy-pyridine-2,6-dicarboxylic acid bis-[(6-amino-4-decyloxy-pyridin-2-yl)-amide] (6): A solution of freshly recrystallized diamine **7** (643 mg, 2.42 mmol) in anhydrous THF (4 mL) was cooled to −78 °C. Butyl lithium was added (2.25 M in hexane, 1.1 mL, 1 equiv) and the solution was allowed to stand at −78 °C for 15 min. A solution of diester **6** (355 mg, 0.42 equiv) in anhydrous THF (3 mL) was then canulated. The reaction was stirred at −78 °C during 4 h and then at romm temperature for 24 h. The reaction was quenched with AcOH (1.2 equiv), and evaporated to dryness. The residue chromatographed on silica gel, eluting with 5/95 Et_3N/EtOAc, to yield 237 mg (28% from **6**) of the product **8** which was immediately used in the following step. ^1H NMR (400 MHz, $CDCl_3$): δ = 10.45 (s, 2H), 7.90 (s, 2H), 7.50 (d, ^4J = 1.6 Hz, 2H), 5.80 (d, ^4J = 1.6 Hz, 2H), 4.49 (br s, 4H), 4.17 (t, ^3J = 6.8 Hz, 2H), 4.01 (t, ^3J = 6.5 Hz, 4H), 1.85 (m, 2H), 1.79 (m, 4H), 1.28 (m, 42H), 0.89 (t, ^3J = 6.8 Hz, 9H).

4-Decyloxy-pyridine-2,6-dicarboxylic acid 2-[(6-amino-4-decyloxy-pyridin-2-yl)-amide] 6-[(6-decanoylamino-4-decyloxy-pyridin-2-yl)-amide] (9): Diamine **8** (237 mg, 0.29 mmol) was dissolved in anhydrous toluene (4 mL) and the solution was cooled to 0 °C. Anhydrous Et*i*Pr_2N (25 μL) was added, followed by freshly distilled decanoyl chloride (30 μL). The reaction was allowed to stand 1 h at 0 °C, then 12 h at room temperature. The mixture was evaporated and purified by chromatography on silica gel eluting with 5/75/20 to 5/55/40 Et_3N/cyclohexane/EtOAc. Some starting material was recovered (132 mg) along with the product (60 mg). IR (thin film): $\tilde{\nu}$ = 3354, 2924, 2854, 1694, 1614, 1580, 1532, 1445, 1349, 1209, 1174, 1049, 852 cm^{-1}; ^1H NMR (400 MHz, $CDCl_3$): δ = 10.34 (s, 1H), 10.30 (s, 1H), 8.33 (s, 1H), 7.89 (s, 2H), 7.70 (d, ^4J = 1.9 Hz, 1H), 7.54 (d, ^4J = 1.9 Hz, 1H), 7.44 (d, ^4J = 1.8 Hz, 1H), 5.76 (d, ^4J = 1.7 Hz, 1H), 4.51 (br s, 2H), 4.16 (t, ^3J = 6.5 Hz, 2H), 4.06 (t, ^3J = 6.5 Hz, 2H), 3.99 (t, ^3J = 6.7 Hz, 2H), 2.35 (t, ^3J = 7.6 Hz, 2H), 1.85 (m, 2H), 1.77 (m, 4H), 1.69 (m, 2H), 1.28 (m, 56H), 0.87 (m, 12H); ^{13}C NMR (200 MHz, $CDCl_3$): δ = 172.5, 168.8, 168.2, 161.6, 161.5, 158.6, 151.3, 150.6, 150.5, 150.3, 149.9, 112.1, 111.9, 97.0, 96.7, 92.9, 90.2, 69.3, 68.5, 68.2, 37.5, 31.9, 29.6, 29.3, 29.0, 28.8, 25.9, 25.8, 25.3, 22.7, 14.1; FAB-MS: *m*/*z* (%): 972.5 (100) $[M]^+$; HRMS (FAB-MS): calcd for $[C_{57}H_{93}N_7O_6+H]$: 972.7266; found: 972.7260.

4-Decyloxy-pyridine-2,6-dicarboxylic acid bis-(6-{[6-(6-decanoylamino-4-decyloxy-pyridin-2-ylcarbamoyl)-4-decyloxy-pyridine-2-carbonyl]-amino}-4-decyloxy-pyridin-2-ylcarbamoyl)-amide (5): 4-Decyloxy-pyridine-2,6-dicarboxylic acid (15.3 mg) and $SOCl_2$ (3 mL) were heated to reflux for 30 min. $SOCl_2$ was distilled off, and the residue was taken up in anhydrous toluene (2 mL) and added to a solution of amine **9** (97 mg) in toluene (1 mL) at 0 °C. The mixture was stirred at room temperature for 12 h. Et_3N (0.5 mL) was added, and the solvent was evaporated. The residue was purified by chormatography on silica gel eluting with 5/95 to 30/70 EtOAc/cyclohexane mixtures, yielding 43 mg of product. M.p. 160–164 °C; IR (thin film): $\tilde{\nu}$ = 3331, 2923, 2854, 1698, 1614, 1583, 1520, 1440, 1337, 1216, 1174, 1123, 1047, 1003, 879, 851, 778, 722, 684, 647 cm^{-1}; ^1H NMR (400 MHz, $C_2D_2Cl_4$, dimer, 1 mM): δ = 10.25 (s, 1H), 10.23 (s, 1H), 10.19 (s, 1H), 9.98 (s, 1H), 9.88 (s, 1H), 9.81 (s, 1H), 7.77 (s, 1H), 7.68 (s, 2H), 7.66 (s, 1H), 7.59 (s, 1H), 7.49 (s, 1H), 7.32 (s, 1H), 7.15 (s, 2H), 7.03 (s, 1H), 6.99 (s, 1H), 6.92 (s, 1H), 6.89 (s, 1H), 6.85 (s, 1H), 6.72 (s, 1H), 6.40 (s, 1H), 4.21 (m, 4H), 4.10 (m, 2H), 3.79 (m, 2H), 3.68 (m, 2H), 3.51 (m, 2H), 3.49 (m, 1H), 3.39 (m, 1H), 1.33 (br m, 140H), 0.93 (m, 21H), 0.86 (t, ^3J = 7.0 Hz, 6H); FAB-MS: *m*/*z* (%): 2232.3 (100) $[M]^+$, 4464.0 (36) $[M_2]^+$.

Acknowledgements

This work was supported by the CNRS, by a predoctoral fellowship (V.B.) from the Forschungszentrum Karlsruhe GmbH and by a post-doctoral NSF-NATO fellowship (R.G.K.). We thank M. Laguerre for assistance with molecular dynamics simulations and A. DeCian and J. Fischer for the use of their X-ray diffraction facilities at ULP, Strasbourg.

[1] P. E. Nielsen, *Acc. Chem. Res.* **1999**, *32*, 624.
[2] D. A Langs, *Science* **1988**, *241*, 188; B. M. Burkhart, R. M. Gassman, D. A. Langs, W. A. Pangborn, W. L. Duax, V. Pletnev, *Biopolymers* **1999**, *51*, 129.
[3] B. Di Blasio, E. Benedetti, V. Pavone, C. Pedone, *Biopolymers* **1989**, *28*, 203.
[4] A. D. McLahan, M. Stewart, *J. Mol. Biol.* **1975**, *98*, 295.
[5] A. Yonath, W. Traub, *J. Mol. Biol.* **1969**, *43*, 461.
[6] H. Kusanagi, *Polymer J.* **1996**, *28*, 708.
[7] a) A. P. Bisson, F. J. Carver, D. S. Eggleston, R. C. Haltiwanger, C. A. Hunter, D. L. Livingstone, J. F. McCabe, C. Rotger, A. E. Rowan, *J. Am. Chem. Soc.* **2000**, *122*, 8856; b) B. Gong, Y. Yan, H. Zeng, E. Skrzypcak-Jankunn, Y. W. Kim, J. Zhu, H. Ickes, *J. Am. Chem. Soc.* **1999**, *121*, 5607; c) H. Zeng, R. S. Miller, R. A. Flowers, B. Gong, *J. Am. Chem. Soc.* **2000**, *122*, 2635.
[8] E. A. Archer, N. T. Goldberg, V. Lynch, M. J. Krische, *J. Am. Chem. Soc.* **2000**, *122*, 5006.
[9] a) J.-M. Lehn, A. Rigault, J. Siegel, J. Harrowfield, B. Chevrier, D. Moras, *Proc. Natl. Acad. Sci. USA* **1987**, *84*, 2565; b) M. Koert, M. Harding, J.-M. Lehn, *Nature* **1990**, *346*, 339; c) R. F. Carina, G. Bernardinelli, A. F. Williams, *Angew. Chem.* **1993**, *105*, *1483*; *Angew. Chem. Int. Ed. Engl.* **1993**, *32*, 1463; d) E. C. Constable, A. J. Edwards, P. R. Raithby, J. V. Walker, *Angew. Chem.* **1993**, *105*, 1486; *Angew. Chem. Int. Ed. Engl.* **1993**, *32*, 1465; for a review see: C. Piguet, G. Bernardinelli, G. Hopfgartner, *Chem. Rev.* **1997**, *97*, 2005.
[10] a) R. Krämer, J.-M. Lehn, A. DeCian, J. Fischer, *Angew. Chem.* **1993**, *105*, *764*; *Angew. Chem. Int. Ed. Engl.* **1993**, *32*, 703; b) B. Hasenknopf, J.-M. Lehn, B. O. Kneisel, G. Baum, D. Fenske, *Angew. Chem.* **1996**, *108*, 1987; *Angew. Chem. Int. Ed. Engl.* **1996**, *35*, 1838; c) B. Hasenknopf, J.-M. Lehn, N. Boumediene, A. Dupont-Gervais, A. Van Dorsselaer, B. Kneisel, D. Fenske, *J. Am. Chem. Soc.* **1997**, *119*, 10956.
[11] a) P. N. W. Baxter, J.-M. Lehn, J. Fischer, M. T. Youinou, *Angew. Chem.* **1994**, *106*, 2432; *Angew. Chem. Int. Ed. Engl.* **1994**, *33*, 2284; b) P. N. W. Baxter, J.-M. Lehn, B. O. Kneisel, D. Fenske, *Angew. Chem.* **1997**, *109*, 2067; *Angew. Chem. Int. Ed. Engl.* **1997**, *36*, 1978; c) P. N. W. Baxter, J.-M. Lehn, G. Baum, D. Fenske, *Chem. Eur. J.* **2000**, *6*, 4510.
[12] T. W. Bell, H. Jousselin, *Nature* **1994**, *367*, 441.
[13] J. Sànchez-Quesada, C. Seel, P. Prados, J. de Mendoza, *J. Am. Chem. Soc.* **1996**, *118*, 277.
[14] a) M. Mascal, C. J. Moody, A. I. Morrell, A. M. Z. Slawin, D. J. Williams, *J. Am. Chem. Soc.* **1993**, *115*, 813; b) I. L. Karle, D. Ranganathan, V. Haridas, *J. Am. Chem. Soc.* **1996**, *118*, 10916; c) A. Rajca, A. Safronov, S. Rajca, R. Shoemaker, *Angew. Chem.* **1997**, *109*, 504; *Angew. Chem. Int. Ed. Engl.* **1997**, *36*, 488; d) K. Nozaki, T. Terakawa, H. Takaya, T. Hiyama, *Angew. Chem.* **1998**, *110*, 138; *Angew. Chem. Int. Ed.* **1998**, *37*, 131.
[15] D. Voet, J. G. Voet, *Biochemistry*, 2nd ed., Wiley, New York, **1995**, pp. 1253.
[16] H. Engelkamp, S. Middelbeek, R. J. M. Nolte, *Science* **1999**, *284*, 785.
[17] a) W. Jaunky, M. W. Hosseini, J.-M. Planeix, A. De Cian, N. Kyritsakas, J. Fisher, *Chem. Commun.* **1999**, 2313; b) S. Hanessian, R. Saladino, R. Margarita, M. Simard, *Chem. Eur. J.* **1999**, *5*, 2169.
[18] V. Berl, I. Huc, R. G. Khoury, M. J. Krische, J.-M. Lehn, *Nature* **2000**, *407*, 720.
[19] V. Berl, I. Huc, R. G. Khoury, J.-M. Lehn, *Chem. Eur. J.* **2001**, *7*, 2798, preceding paper in the present issue.
[20] This marked effect may result form a larger number of interactions between the side chains as well as an increase in the interactions between aromatic rings due to the electron donor character of the decyloxy substituent in **5**.

  0947-6539/01/0713-2819 $ 17.50+.50/0

[21] S. M. Redmore, C. E. F. Rickard, S. J. Webb, L. J. Wright, *Inorg. Chem.* **1997**, *36*, 4743.
[22] Water could never be completely removed.
[23] The H-O-H angle of the water molecules is considerably opened to 160°. The O–H bonds are thus almost aligned with the helix axis preventing the water hydrogens to form hydrogen bonds to the pyridine nitrogens of the strands. The water oxygens are within hydrogen bond distance to two amide hydrogens (2.99 Å but NH ··· O angles of only 137° are unfavorable for a strong interaction.
[24] Some of these hydrogen bonding motifs are also found in the crystal structure of the related compound *N*,*N*′-bis-(6-methyl-pyridin-2-yl)-isophtalamide: M. Mazik, D. Bläser, R. Boese, *Tetrahedron* **1999**, *55*, 12771.
[25] For a detailed discussion of this structural dissymmetry, and its dynamics in solution, see ref. [18].
[26] The two strands of each duplex are crystallographically inequivalent. Thus, this structure represents an example of the co-crystallization of two different conformers of the same compound as seen in Gramicidin crystals and in steroids. See: a) B. M. Burkhart, N. Li, D. A. Langs, W. A. Pangborn, W. L. Duax, *Proc. Natl. Acad. Sci. USA* **1998**, *95*, 12950; b) H. Campsteyn, O. Dideberg, L. Dupont, J. Lamotte, *Acta Crystallogr. Sect. B* **1979**, *35*, 2971.

Received: January 8, 2001 [F2990]

  0947-6539/01/0713-2820 $ 17.50+.50/0